Visualising complex morphology of fatigue cracks in voxel based 3D datasets

B. Müller*[1], F. Pfrunder[1], L. Chiocca[1], N. Dorin Ruse[2] and F. Beckmann[3]

Fatigue cracks are usually characterised by surface sensitive techniques after specimen failure. High resolution micro computed tomography (μCT) based on synchrotron radiation allows the non-destructive visualisation of crack morphology and evaluation of fatigue crack formation/propagation before specimen failure. The visualisation of the complex fracture morphology with characteristic features out of the acquired set of slices is, however, challenging. To obtain a reasonable estimate, two approaches are generally used: the determination of mass centre points in the hollow space and the minimum intensity search in parallel projections. The more sophisticated approach using the elastically deformable contour model, the physical analogy of a rubber band, termed snakes, gives rise to crack morphologies with much less artefacts. The approach was used in the present study for the characterisation of fatigue cracks in poly(methylmethacrylate) (PMMA) and a dental ceramic. The search for the appropriate snake parameters works much better for homogeneous materials, here PMMA, than for inhomogeneous materials, here a dental ceramic. For the ceramic, the regions where the snakes approach provided reasonable results were restricted. Combining μCT with sophisticated computer vision techniques enables the unique characterisation of cracks at the micrometre scale.

Keywords: Microtomography, Fatigue crack, Crack morphology, Elastically deformable contour model

Introduction

The remodelling process present in some hard tissues, such as bone, can repair microcracks. Since such a process has not yet been implemented in biomaterials, the study and characterisation of fatigue microcracks could play an important role in their life prediction. Micro computed tomography (μCT) is a non-destructive, three-dimensional (3D) method of micrometre resolution that could greatly facilitate such studies. The analysis of the huge 3D datasets generated by μCT, usually of gigabyte size, cannot be performed using commercially available software but needs the development and implementation of sophisticated algorithms. Combining high resolution μCT with sophisticated image analysis could allow the accurate determination of crack length to enable the accurate determination of the rate of crack propagation and therefore the accurate determination of the fatigue behaviour of the material to be optimised. Such measurements should also provide the crack morphology with isotropic spatial and density resolution in the three orthogonal directions, which can be used in the investigation of the failure mechanism. Therefore, these rather time consuming precision measurements could be used to validate and/or calibrate other less sophisticated methods currently used for the crack length determination and the non-destructive morphology characterisation.

The first problem to be mastered is the detection of the cracks in the tomogram. Using the absorption contrast mode, the crack has to be thick enough to significantly reduce the absorption in the related voxels.[1] Inhomogeneity of the material, all kinds of artefacts, and the noise in the tomogram complicate the crack detection. To segment the cracks, an appropriate threshold for the region of interest has to be chosen, although a certain tolerance exits.[2]

Even though the first problem is mastered, the crack has to be visualised on the basis of the tomogram, which could be especially difficult for the composite type materials used in dentistry. In the simple two-dimensional (2D) slices, the crack may be detectable but its 3D morphology is hardly seen, if just state of the art volume rendering is applied.[3] An algorithm is required, which detects the coordinates of all voxels belonging to the crack. Because of artefacts and noise, however, many voxels, which are outside the crack, exhibit the same local absorption but have to be eliminated. More importantly, often only a part of the crack is identified, because the crack can be closed in certain regions.[3] Therefore, the authors propose to use the active contour model,[4] which is based on a physical analogy: the energy of a rubber band, termed 'snake',

[1]Computer Vision Laboratory, ETH Zurich, Sternwartstr. 7, 8092 Zürich, Switzerland
[2]Faculty of Dentistry, University of British Columbia, Vancouver, V6T 1Z3, Canada
[3]Institute for Materials Research, GKSS-Research Centre Geesthacht, Max-Planck-Str. 1, 21502 Geesthacht, Germany

*Corresponding author, email bmueller@vision.ee.ethz.ch

Published by Maney on behalf of the Institute
Received 30 January 2006; accepted 19 April 2006
DOI 10.1179/174328406X114162

with certain properties is minimised adjusting the one-dimensional (1D) band line wise to the detected crack voxels. This approach needs the identification of the appropriate snake parameters, which finally allow for convergence.[5]

Materials and methods

Notchless triangular prism fracture toughness tests

Fracture toughness tests belong to the standard engineering procedures to characterise dedicated materials. Different testing and specimen designs have been introduced to determine the fracture toughness of dental materials including calcium hydroxide preparations,[6] denture base acrylic resins,[7] dental ceramics[8] and composites,[9] cements and various adhesive interfaces.[10] These studies have also incorporated the effect of the environment, thermal cycling and cyclic fatigue on the fracture toughness.

The chevron notched short rod (CNSR) configuration introduced by Barker[11] and modified by Pilliar *et al.*[12,13] is especially suited for fracture toughness tests of brittle materials. The test involves a relatively small sample prepared by cutting a chevron notch in a cylindrical specimen. This process is cumbersome and difficult to control, especially with small samples of very brittle materials such as dental ceramics. It is even more complex and prone to error when used to characterise bonded interfaces. Therefore, the notchless triangular prism fracture toughness test has been developed and validated through finite element analysis.[14] The objective was to retain the overall geometry of the CNSR but to avoid the cumbersome notching procedure. This procedure simply uses the notchless triangular prism specimen, which is fixed in the holder to achieve the CNSR configuration.

A sharp blade helps to create an about 0·1 mm deep crack initiation point midway along one of the prism edges. The test assembly, prism and holder, is secured in the custom designed grips and attached to the computerised universal testing machine (Instron model 4301, Instron Canada Inc.). An extensometer is attached between the lips of the grips. The assembly is loaded in tension at a crosshead speed of 0·1 mm min^{-1}, and the load and the displacement are constantly monitored and recorded. Hence, well defined conditions to introduce fatigue cracks into the prism are realised.

If the prism is transparent, optical techniques can be used to follow the crack formation. If, however, the specimen is opaque, the crack formed can only be made visible after specimen failure. Figure 1 shows photographical and SEM images of fatigue fractured surfaces in a failed specimen. The initiation point and characteristic rough and flat areas are visible.

Synchrotron radiation based micro computed tomography

Synchrotron radiation based μCT (SRμCT) in absorption contrast mode is well established to quantitatively characterise the 3D structure of different kinds of materials and the anatomy of various human tissues with true micrometre resolution. The main advantage with respect to conventional μCT is the much higher

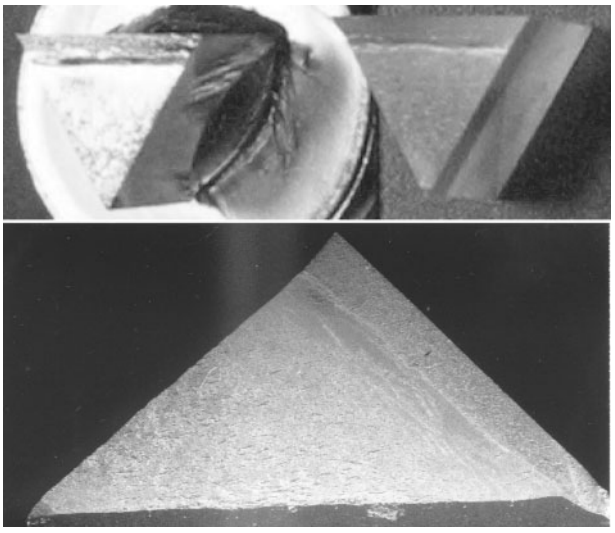

1 Photograph of fatigue crack in PMMA after destruction of specimen is shown in the upper part; on left hand side, specimen is gold coated; this is used for secondary electron microscopy represented in lower part; here, initiation point (left corner), different characteristic zones of fatigue crack and, opposite to initiation point, trapeziform surface of break, which was generated after SRμCT data acquisition, can clearly be identified

photon flux, which offers to eliminate all photons but the ones of desired energy, and still maintain a reasonable period of time for data acquisition. Bragg reflection by single crystals permits the realisation of a tuneable X-ray source. Because the X-ray absorption coefficient μ strongly depends on both energy E and atomic number Z, the choice of the photon energy can be optimised minimising the total exposure time at any prescribed sensitivity by the relationship $\mu(E,Z)D=2$, where D corresponds to the average sample diameter, as shown by Grodzins.[15] Therefore, for the present study, photon energies of 11 and 24 keV were selected for the investigation of poly(methylmethacrylate) (PMMA) and ceramic specimens respectively. The spatial resolution was determined by the modulation transfer function of an edge of a gold plate recorded under the conditions applied for the data acquisition[16] and corresponds to 8·0 and 5·2 μm for the PMMA and ceramic specimens respectively. Note that the voxel lengths were chosen to 5·0 and 3·3 μm because of the different specimen cross-sections.

The experiments were carried out at the beamline BW2 (Hasylab at DESY) taking advantage of the standard set-up for tomography.[17] The fixed exit double crystal monochromator Si(111) provides the monochromatic X-ray beam of desired energy and necessary flux. The sagittally bent second Si(111) crystal reduces the beam divergence and forms a parallel beam about 10 mm wide and 3 mm high.

This beam is partly absorbed in the sample and generates the projection image on the fluorescence screen (200 μm thick $CdWO_4$ single crystal). After moderate magnification, the image is mapped on a Kodak KAF 1600 CCD chip (1536 × 1024 pixels, pixel length 9 μm) and acquired using 14 bit digitalisation at a frequency of 1·25 MHz. In the present study, 361 projections were recorded by rotating the sample in steps of 0·5° from 0 to 180°. In order to eliminate the beam

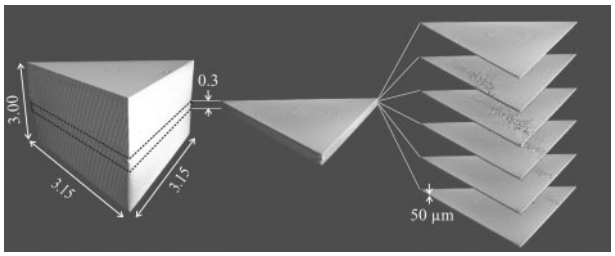

2 Acquired tomogram has height of 3 mm; since crack in PMMA specimen is located within height of ~0·4 mm, amount of data can be reduced to region of interest, i.e. triangular specimen cross-section and a stack of 76 slices each 5 μm thick, which is reduction of more than one order of magnitude (to 113 MB); on right, location of crack is made visible using slices 50 μm thick; individual slices, however, do not provide crack morphology, which would allow drawing conclusions on crack origin and formation

non-uniformities and account for the detector noise, the difference between the individual bare projections and the dark image was divided by the difference of the beam and the dark image to obtain the corrected projections, which were the basis of the slice by slice reconstruction performed with the filtered back projection algorithm.[18] Nevertheless, image inhomogeneities still existed owing to the photon counting statistics and prominent defects in the fluorescence screen.

Results

Selection of region of interest

The crack started from the crack initiation point and was directly observed on the specimen's surface. This knowledge helped to identify the crack within the voxel based 3D dataset. Using homogeneous materials, it is rather simple to determine the location of the crack inspecting individual slices, as shown in Fig. 2. Hence, the amount of data for the PMMA specimen with a tomogram size of 1·5 GB could be reduced to 113 MB and for the ceramic specimen with a tomogram size of 2·5 GB to 68 MB, which is a reduction of more than one order of magnitude. The datasets can be even further reduced, taking into account the triangular cross-section of the specimens used.

Intensity based segmentation

Intensity based methods for segmentation belong to the simplest approaches to extract details with defined properties out of the 3D dataset. Voxels belonging to the crack should have lower absorption than the surrounding material. If this difference in absorption is high enough on the length scale of resolution, the crack becomes light. *A priori*, one cannot assume that the product of the width of the crack and the difference in absorption between air and material are sufficient. The data of both PMMA and ceramics clearly demonstrate that even without the use of any contrast agent or preloading, the crack is clearly identified.

In order to segment the crack, the threshold for the absorption has to be determined. The tomograms acquired at the beamline BW2 lead to peaks in the absorption histograms of perfect Gaussian shape.[19] For a two component system (air–material), two Gaussians

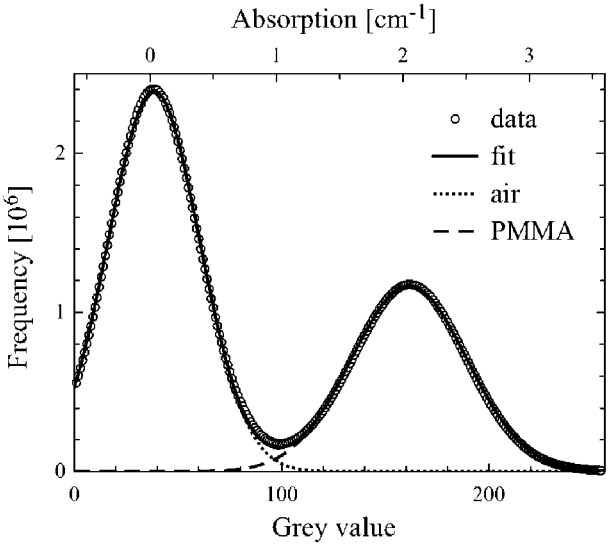

3 Because PMMA specimen is homogeneous, absorption histogram just exhibits two peaks (material and air) and certain amount of partial volume effects between them; peaks are well separated; consequently, threshold for intensity based segmentation can be set to crossing point of both Gaussians

accurately describe the histogram as shown in Fig. 3. The slightly higher values between the two peaks are the result of partial volume effects. Because both peaks are well separated, the crossing point of the two Gaussians between grey values 96 and 97, which is not the minimum between both (grey value 98), is the best choice for the threshold.[19] Thus, all voxels with a local absorption represented by grey values up to 96 are set to air, whereby the voxels with a local absorption associated with values beginning from 97 are set to PMMA. This binarisation further reduces the size of the dataset and makes easier the identification of the crack. Nevertheless, the thresholding does not allow identifying the crack in a unique manner.

Artefacts and noise in SRμCT

The snake algorithm does not suitably work, if too many ring-like artefacts are present. These artefacts result from defects in the fluorescence screen and give rise to dark or bright spots in the acquired images. They become more numerous during the lifetime of the screen and cannot be fully avoided. The present study was performed at the end of the lifetime of the screen and the number of ring-like artefacts was relatively large. Several codes have been developed to process the data with the aim to remove these artefacts replacing the related pixels or voxels by reasonable estimates.[20] The defects in the projections are independent on the rotation angle and thus show up as lines in the sinogram. The authors have automatically replaced most of these lines averaging the pixels from the left and the right. Although this approach does not remove all artefacts, it considerably reduces their number.

Line and star artefacts caused by strongly absorbing particles within the specimen are rare. Hence these artefacts do not influence the applicability of the snake algorithm.

Besides the artefacts, noise increases the problems in the analysis of tomograms. Figure 3 shows a broadening

of the air and PMMA peaks with minor overlap. The noise is the result of the photon statistics. It is possible to reduce the noise, increasing the exposure time. The benefit, however, becomes smaller and smaller. Even more important are restrictions from the camera chip, which only allows counting until 16 k. Therefore, a significant level of noise is even present for homogeneous materials. Sophisticated algorithms have to be applied in order to extract the required information.

Elastically deformable contour models (snakes): 1D elastic structure

The non-rigid shape models start from an initialisation of an approximate contour, which is usually a rough estimate. Subsequently, the contour is automatically adjusted to the image structures. A regularisation is required to avoid any over fitting during the automatic adjustment, especially important when the images are noisy. In order to extract the crack out of a 2D image, the physical analogy of a rubber band can be used, which is moved under the influence of two forces: first, the image force F_i that pushes the band towards the crack and second, the elastic forces F_d of the band that avoid too strong expansions and bending, therefore preventing the over fitting to low scale noisy structures. The simple linear elastic behaviour is sufficient for the deformable contour models. The difficulty lies in the selection of the arc length s dependent parameters, i.e. tension $\alpha(s)$, rigidity $\beta(s)$, damping $\gamma(s)$ and mass $\mu(s)$ of the snake. It should be noted that the target is a reasonable local minimum and not the global minimum, because the rubber band has a tendency to shrink, and zero energy would be reached by shrinking the band to any single point. Another problem to be solved is the appropriate choice of the boundary conditions. Since the crack can accurately be determined on the surface, it is reasonable to fix the band at the exit of the crack, i.e. (x_1,y_1) and (x_2,y_2). The problem can be formulated for a rubber band in 2D space using the energy based description, depending on the image attractors by means of the related potential field $P(x,y)$

$$E_I(\vec{x}) = -\iint_{x,y} P(x,y)\,dx\,dy$$

$P(x,y)$ is only a function of the image, but there is no unique choice. Following the usual way, the magnitude of the image gradient is applied here.

The deformation energy E_d, which represents the resistance of the rubber band against bending and stretching, enforces the smoothness of the band. The two linear contributions are the tangential stretching, i.e. the first derivative of s, and the bending, i.e. the second derivative of s

$$E_D(\vec{x}) = \frac{1}{2}\int_s \left[\alpha(s)\left|\frac{\partial\vec{x}}{\partial s}\right|^2 + \beta(s)\left|\frac{\partial^2\vec{x}}{\partial s^2}\right|\right] ds$$

whereby $\vec{x}(s,t) = [x(s,t),y(s,t)]$ with t being the time.

The total energy on the band (snake) to be optimised deforming the snake in time is therefore

$$E[\vec{x}(s,t)] = E_D[\vec{x}(s,t)] + E_I[\vec{x}(s,t)]$$

Often it is necessary to add further energy terms, which are also needed to give the band the physically meaningful behaviour.[5] First, the kinetic energy E_k is introduced

$$E_k = \frac{1}{2}\int_s \mu(s)\left|\frac{\partial\vec{x}(s,t)}{\partial t}\right|^2 ds$$

Second, the friction or damping energy E_F is necessary to address the energy dissipation, e.g. modelled through the Rayleigh functional

$$E_F(\vec{x}) = \frac{1}{2}\int_s \gamma(s)|x_t|^2 ds$$

Damping related to the energy dissipation does not only lead to the realistic rubber band (snake) behaviour, but especially improves the condition of the stiffness matrix through the diagonal term. Over damping, however, is undesirable because the snake is glued and does not allow moving.

The snake motion is calculated, minimising the following integral

$$\int_s [E(\vec{x}) + E_k(\vec{x}) + E_F(x_t)]\,ds \rightarrow \min.$$

For the numeric solution, finite differences and the boundary conditions mentioned above were used. Smoother image potentials, which simplify the calculation, can be created implementing appropriate filters.

If the tomogram is not well prepared for the snake algorithm, i.e. without the removal of the numerous ring-like artefacts, the image potential is not strong enough to give rise to satisfactory results. Figure 4*a* shows that the snake fits the crack well if the snake is in the direct ($\sim$20 to 30 μm) neighbourhood of the crack. If the starting location is not close enough and noisy structure and artefacts are present, the algorithm does not converge towards a reasonable result. Any improvement cannot really be found between iteration steps 150 and 300. The variation of the snake parameter does not yield significantly better results. Hence, for noisy structures rich in artefacts, the model has to be further improved.

It is known that additional energy terms can globally influence the snake behaviour in a positive manner. Here, a kind of gravitation has been introduced, which forces the snake to move into a predefined direction, namely towards the crack. After removal of the ring-like artefacts and applying the additional force, the snake automatically detects the crack in the 2D image within only some 10 iteration steps, as shown by the image sequence in Fig. 4*b*.

Elastically deformable surfaces

The basic idea of the 1D rubber band can be generalised to 2D membranes to detect the crack morphology. One of the simplest solutions is to build the membrane out of a finite number of equivalent elastic bands in parallel fashion. Such a membrane once obtained can be used to make visible the crack and to quantify its features.

In order to demonstrate that the snake algorithm provides better results than the state of the art estimates, the authors have implemented two approaches for the specimens: the mass centre point method and the minimal intensity method. The minimal intensity approach transforms the 3D dataset into a 3D height

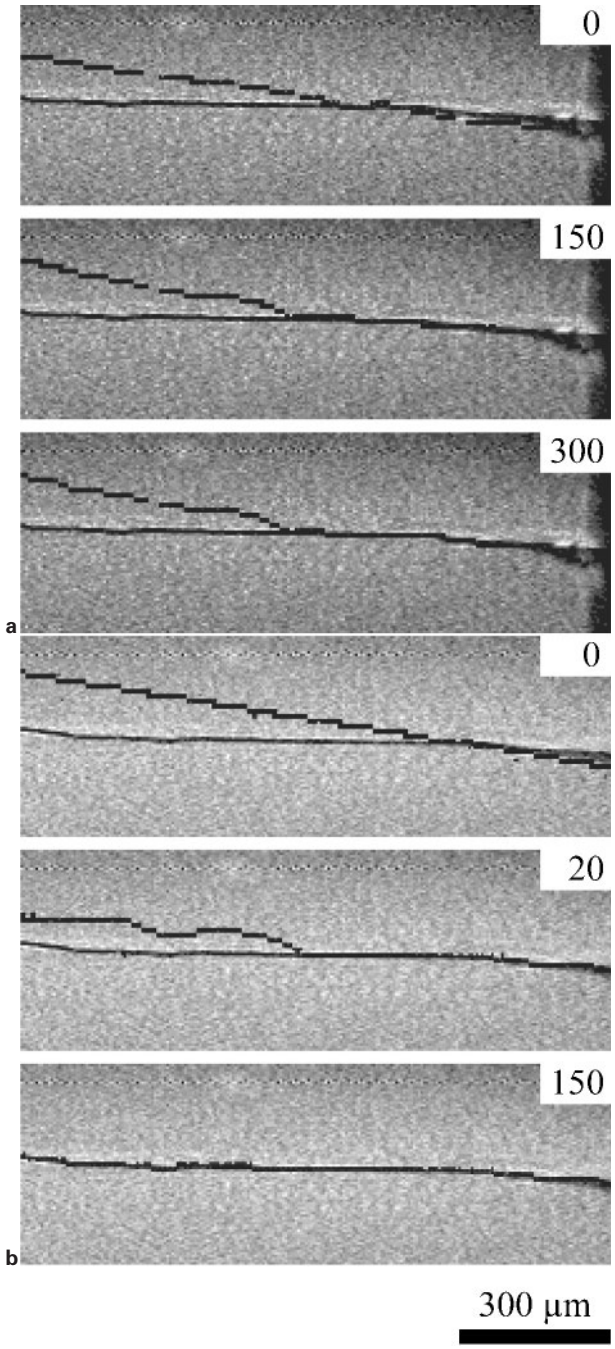

a only image potential; *b* added driving force

4 In general, snake algorithm is applied to lines in two-dimensional manner as demonstrated here; in *a*, grey values of pixels give rise to potential, which forces snake towards crack; obviously, this potential is not strong enough to identify crack; therefore, driving force is added; together with further improvements such as artefact reduction, this approach even allows choice of less suitable starting values but to guarantee unique identification of crack in two dimensional data-set; number of iteration steps is indicated

field, using a ray tracer. The visualisation of the crack using the minimal intensity approach can also be realised by the ray casting.[21] The simple initialisations, including ray casting, are not enough to obtain the desired crack morphology in a quantitative manner, although meaningful representations of restricted areas of rather homogeneous specimens are reported.[2]

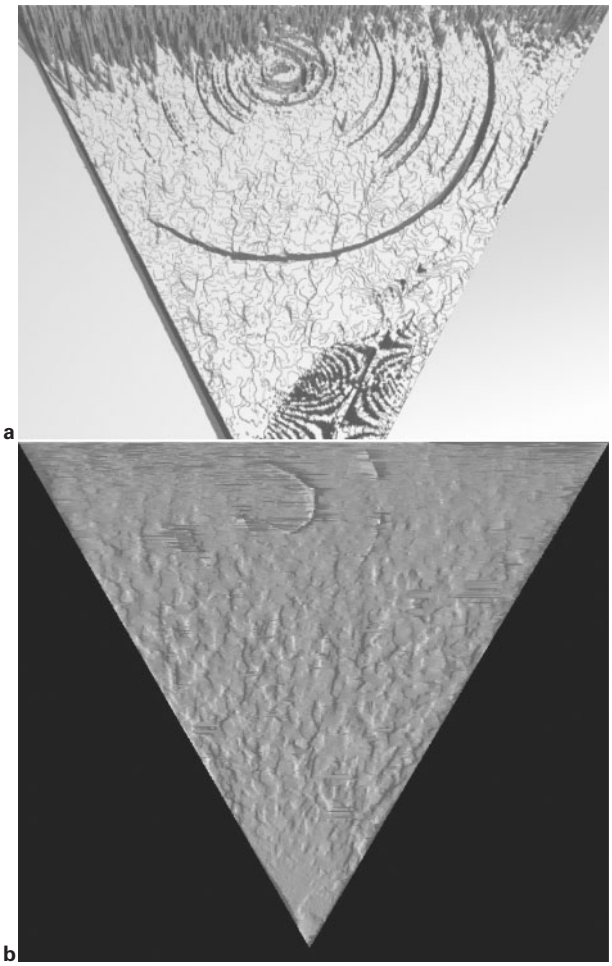

a minimal intensity; *b* snakes

5 For homogeneous materials, simple approaches such as visualising minimal intensity voxels in projection plane enable extraction of many details (cf. *a*); snake algorithm, however, results in rather smooth images with only very few artefacts, because artefacts located sufficiently far from crack are eliminated

Following the mass centre point method, the authors have searched for neighbouring 'air' voxels to be labelled. The mass centre points of the identified clusters should allow generating the approximated crack surface. The size of the identified clusters should be restricted to suppress the area outside the PMMA specimen and, more importantly, to avoid the incorporation of the numerous artefacts. In order to avoid the incorporation of clusters, which are generated because of noise, a minimal cluster volume should also be set. Using a minimal cluster volume of 20 voxels and a maximal volume of 100 voxels, the number of points has been reduced from 3127 to 2005. Although this approach yields interpolation values of the crack, their density is inappropriate to visualise the characteristic crack features.

Better results are obtained by the minimal intensity method, although several steps using conventional software were necessary. In the first step, the height field and the intensity image have been produced respectively, which already provide an idea of the crack morphology.[22] In order to improve the visualisation, the grey values below the threshold (cf. Fig. 3) are set to zero. Of course, the results are much better after the

removal of ring-like artefacts. Noise is reduced by the application of a median filter, or even better by the use of the 'dust and scratch removal' filter of Adobe Photoshop. Finally, POV Ray was chosen to visualise the height field, as shown in the upper part of Fig. 5. In the central part, many fine details are visible. Hence, this approach leads to images, which can be used, besides the SEM images, for the validation of the snakes approach. Please note, however, that additional artefacts occur in the marginal zones. The estimate is only locally helpful and the artefacts, especially the strong ring-like artefacts, are pronounced.

The snake approach of the elastic band is linewise generalised to the elastic membrane. Although the additional force in y direction is very supportive, the selection of the parameters is still time consuming. One of the results is shown in Fig. 5*b*, where the tension is set to 26, the rigidity to 9, the mass of the snake to 30 and the damping to 1 (Ref. 22). It has been realised that the choice of the threshold is important for the success of the authors' approach. During the iterations, the convergence of the snake has been observed in three planes perpendicular to the crack. This enabled the authors to decide on the termination of the programme and to search for the most appropriate snake parameters. The image in Fig. 5*b* clearly demonstrates that the application of the snake algorithm considerably reduces the artefacts visible in the minimal intensity method images but conserves the crack features of micrometre size.

Discussion and conclusions

The application of the snake algorithm using an elastic membrane to be adapted to the SRμCT data allows the non-destructive visualisation of the crack morphology with micrometre resolution. Because the data are acquired non-destructively without any use of contrast agent, the crack propagation can be followed in time. The limitation is the amount of data generated, i.e. several gigabytes per step and the time consuming data analysis. It is expected, however, that once the appropriate procedures and parameters are identified, the data analysis becomes straightforward. As shown in Fig. 6, SEM images show much more details with respect to SRμCT data owing to the higher lateral spatial resolution. Therefore, the combination of SRμCT and sophisticated 3D data analysis will not replace the SEM images of cracks, which are obtained after the specimen is fractured, but will be rather complementary. Please note that the quantification of the crack morphology by the use of SEM images[23] is a very expensive task, too, and the membrane, which contains the features with equidistant resolution in the three orthogonal directions on a micrometre scale, can help to calibrate the approximations calculated from the SEM images.

For the homogeneous specimen such as PMMA, the approach works in an automatic way. For dental composites, however, the estimate to initialise the snakes has to be found within restricted volumes mainly manually. Another limitation of the authors' approach is that multiple, branching cracks can only be handled in subvolumes, where just one single crack is present.

Concerning morphology representation, the approach has the problem to round the edges of the crack. In order to obtain the desired replica of the crack, the snake parameters have to be carefully selected.

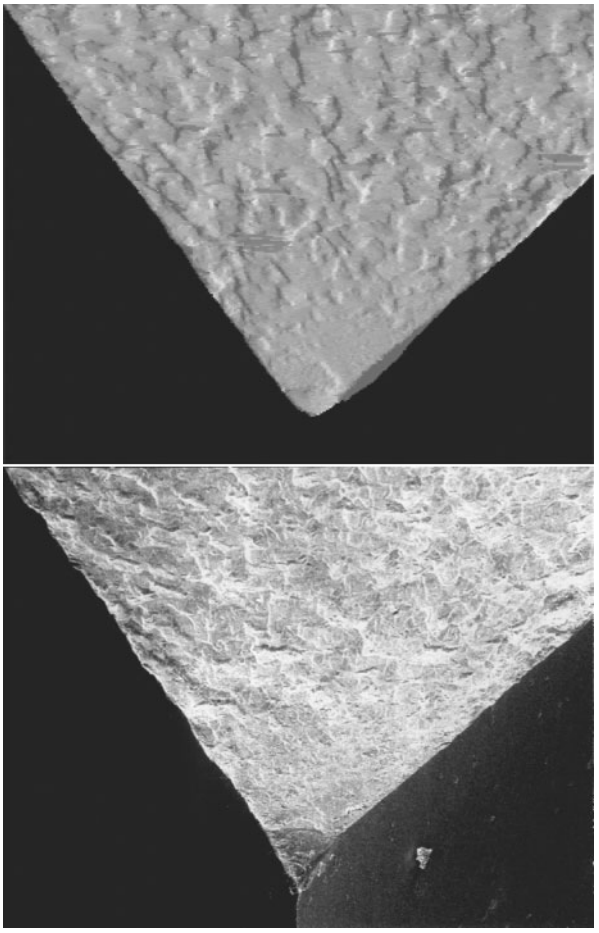

a SRμCT and snakes; *b* electron microscopy

6 Snake algorithm applied to SRμCT data only enables visualisation of features with sizes larger than spatial resolution, i.e. here 9 μm; SEM yields, therefore, much more details; because SEM images of crack surface can only be obtained after specimen failure, both methods are complementary; crack formation, followed by SRμCT, can be subsequently validated by use of SEM images

It should be noted that the synchrotron radiation source used in the present study belongs to the second generation. Therefore, the prominent edge enhancement on the crack surfaces ('Schlieren' type) due to the coherence of the X-rays from the third generation sources[3] is mainly suppressed. Because of the restricted numbers of photons, however, the noise level might be higher for the tomography using second generation synchrotron radiation sources. Toda *et al.*[2] pointed out that noise and artefacts, which are directly reflected in the quantitative results such as crack opening, are not specifically described in the literature. Consequently, the presented quantitative data are somehow questionable, especially if subvoxel interpolation is integrated.

Intensity based segmentation algorithms rely on the appropriate choice of the threshold. The rather simple estimates work only for very specific cases. The choice of Lee *et al.*[24] is too simple, because their histogram presented does not exhibit two peaks of identical amplitude and width. This might be also the reason why they subsequently presented a different approach.[1]

The sensitivity analysis, as given by Toda *et al.*,[2] does not yield the optimal choice for the threshold, but shows that the feature detection and its robust measurement are relatively independent on the thresholding conditions. In a previous paper,[19] the authors have demonstrated that the absorption histograms of tomograms generated at the second generation synchrotron have a perfect Gaussian distribution and allow determining the threshold from the crossing point of the two Gaussians, if two distinct peaks are present. The broadening of the peaks is often correlated with the noise, which complicates the visualisation of the features of interest (here the crack) just using the intensity based segmentation procedures. Especially for medical imaging, knowledge based algorithms are developed. Since it is assumed that the crack forms a 2D object with well defined boundary conditions and without any bifurcation in the region of interest, the authors' approach belongs to the knowledge based procedures.

Despite the numerous difficulties and the rather expensive data preparation for the application of the snakes to the fatigue crack, the combination of the non-destructive 3D visualisation by SRμCT and highly sophisticated computer vision methods using elastically deformable contour models enables the accurate determination of the fatigue behaviour of the material to be characterised and optimised.

Acknowledgements

The authors are grateful to Gábor Szekely, who provided the idea to apply the snake algorithm to visualise the crack, and acknowledge the support of Philipp Thurner during the data acquisition. This contribution is based on a presentation at the International Workshop on 'Applications of X-ray tomography to study fracture and crack growth' held at Churchill College, Cambridge, UK in April 2005. The workshop was supported by Office of Naval Research Global under Department of the Navy Grant No. N00014-05-1-1043. The United States Government retains a royalty free license throughout the world in all copyrightable material contained herein.

References

1. A. Guvenilir, T. M. Breunig, J. H. Kinney and S. R. Stock: *Acta Metall.*, 1997, **45**, 1977.
2. H. Toda, I. Sinclair, J.-Y. Buffiere, *et al.*: *Philos. Mag.*, 2003, **83**, 2429.
3. A. Steuwer, L. Edwards, S. Pratihar, *et al.*: *Nucl. Instrum. Meth. Phys. Res. B*, 2006, **246B**, 217.
4. M. Kass, A. Witkin and D. Terzopoulos: *Int. J. Comput. Vision*, 1988, **1**, 321.
5. W. Neuenschwander: 'Elastic deformable contour and surface models for 2-D and 3-D image segmentation'; 1996, Konstanz, Hartung-Gorre Verlag.
6. C. H. Lloyd and J. N. Anderson: *J. Oral Rehabil.*, 1980, **7**, 155.
7. G. D. Stafford, R. Huggett and B. E. Causton: *J. Biomed. Mater. Res.*, 1980, **14**, 359.
8. K. Kvam: *Biomaterials*, 1992, **13**, 101.
9. R. M. V. Pidaparti, W. A. Boehmer and M. W. Beatty: *Eng. Fract. Mech.*, 1993, **45**, 51.
10. L. E. Tam and R. M. Pillar: *J. Dent. Res.*, 1993, **72**, 953.
11. L. M. Barker: *Eng. Fract. Mech.*, 1977, **9**, 361.
12. R. M. Pillar, D. C. Smith and B. Maric: *J. Dent. Res.*, 1986, **65**, 1308.
13. R. M. Pillar, R. Vowles and D. A. Williams: *J. Biomed Mater. Res.*, 1987, **21**, 145.
14. N. D. Ruse, T. Troczynski, M. I. MacEntee and D. Feduik: *J. Biomed. Mater. Res.*, 1995, **31**, 457.
15. L. Grodzins: *Nucl. Instrum. Meth.*, 1983, **206**, 541.
16. B. Müller, P. Thurner, F. Beckmann, *et al.*: in 'Developments of X-ray tomography III', (ed. U. Bonse), Vol. 4503, 178; 2001, San Diego, CA, SPIE.
17. F. Beckmann: in 'Developments in X-ray tomography III', (ed. U. Bonse), Vol. 4503, 34; 2001, San Diego, CA, SPIE.
18. A. C. Kak and M. Slaney: 'Principles of computerized tomographic imaging'; 2001, Philadelphia, PA, Society of Industrial and Applied Mathematics.
19. B. Müller, F. Beckmann, M. Huser, *et al.*: *Biomol. Eng.*, 2002, **19**, 73.
20. J. Sijbers and A. Postnov: *Phys. Med. Biol.*, 2004, **49**, N247.
21. S. D. Roth: *Comput. Graph. Image Process.*, 1982, **18**, 109.
22. F. Pfrunder and L. Chiocca: 'Computer vision lab, electrical engineering and information technology'; 2004, Zürich, ETH Zurich.
23. E. Ponz, J. L. Ladaga and R. D. Bonetto: *Microsc. Microanal.*, 2006, **12**, 170.
24. S.-B. Lee, S. R. Stock, M. D. Butts, T. L. Starr, T. M. Breunig and J. H. Kinney: *J. Mater. Res.*, 1998, **13**, 1209.